Original Article
pISSN 1738-2637
J Korean Soc Radiol 2012;67(5):371-380

대한영상의학회지

Dual Energy Computed Tomography to Evaluate Hepatocellular Carcinoma Treated with Transcatheter Arterial Chemo-Embolization: Comparison between the Linear Blending and Nonlinear Moidal Blending Methods[1]

경도관동맥화학색전술로 치료받은 간세포암의 평가에 있어 이중에너지 CT: 선형혼합기법과 비선형 Moidal 기법의 비교[1]

Sang Soo Shin, MD[1], Heoung Keun Kang, MD[2], Hyeong Wook Kim, MD[1], Jin Woong Kim, MD[2], Suk Hee Heo, MD[2], Yong Yeon Jeong, MD[2], Hyun Ju Seon, MD[2], Daun Lee, MD[1]

[1]Department of Radiology, Chonnam National University Hospital and Medical School, Gwangju, Korea
[2]Department of Radiology, Chonnam National University Hwasun Hospital and Medical School, Hwasun, Korea

Purpose: To compare the linear blending image with the nonlinear moidal blending image using dual energy CT for the evaluation of the viable portion of hepatocellular carcinoma (HCC) after transcatheter arterial chemoembolization (TACE).

Materials and Methods: One-hundred and twenty three HCC patients incompletely treated after TACE were enrolled in this study. The dual energy mode (80 kVp and Sn140 kVp) was only applied in the late arterial phase scanning. A paired *t*-test was used to compare the lesion-to-liver contrast-to-noise ratio (CNR) and the image noise between the two blending images. Lesion conspicuity, image sharpness, image noise and the overall image quality between the two blending images were compared using the Wilcoxon matched-pair signed-ranks test.

Results: The lesion-to-liver CNR was significantly higher on the moidal blending image (5.6 ± 3.2) than on the linear blending image (2.7 ± 1.6) ($p < 0.001$). The image noise was significantly lower on the moidal blending image (10.9 ± 3.5) than on the linear blending image (17.5 ± 5.5) ($p < 0.001$). The lesion conspicuity and overall image quality were significantly better on the moidal blending image for both reviewers ($p < 0.001$). However, with respect to image sharpness, the linear blending image was significantly better for both reviewers ($p < 0.01$).

Conclusion: The nonlinear moidal blending image of dual energy CT showed an increased lesion-to-liver CNR, decreased noise and improved overall image quality for the evaluation of the viable portion of HCC after TACE.

Index terms
Liver
Hepatocellular Carcinoma
Dual Energy CT
Image Fusion
Chemo-Embolization

Received July 11, 2012; **Accepted** August 17, 2012
Corresponding author: Heoung Keun Kang, MD
Department of Radiology, Chonnam National University Hwasun Hospital and Medical School, 322 Seoyang-ro, Hwasun-eup, Hwasun 519-763, Korea.
Tel. 82-61-379-7101 Fax. 82-61-379-7133
E-mail: hkkang@jnu.ac.kr

This study was supported by a grant (CRI12013-1) from the Chonnam National University Hospital Research Institute of Clinical Medicine in South Korea.

INTRODUCTION

Transcatheter arterial chemoembolization (TACE) has been widely used as one of the alternatives to surgical treatment for patients with hepatocellular carcinoma (HCC) (1-4). Although it has been reported to improve the rate of survival (5, 6), TACE is still regarded as a bridge to liver transplantation or a palliative treatment for patients with unresectable HCC (7). In general, TACE should be repeatedly performed in order to make HCC completely necrotic without any remaining viable portion. Thus, the treatment response after TACE is routinely evaluated with various imaging modalities, such as CT, contrast-enhanced ultrasonography and magnetic resonance imaging (MRI) in order to determine whether subsequent sessions of TACE need to be performed (3).

Although there has been no obvious agreement regarding which imaging technique is superior to others for evaluating

the therapeutic response after TACE (2, 8), CT has been mainly used as the fundamental imaging tool for monitoring the tumor response in patients with HCC after TACE (1, 3, 4, 9). CT has the ability to reveal the degree and pattern of accumulation of iodized oil within the mass as well as the presence of the viable portion of HCC after TACE (1). Among the various phases of the contrast-enhanced CT, the hepatic arterial phase can play a pivotal role in detecting a residual viable tumor or recurrent tumor within or around the iodized oil-retaining tumor (10). That is, if arterial hypervascularity within or around the iodized oil-retaining tumor is seen during the hepatic arterial phase, then this lesion is presumed to be a possible viable portion of a tumor. However, the accurate identification of a viable tumor in follow-up CT after TACE for treating HCC is not always promising (4, 9). Generally, the ability of CT to evaluate the HCC in which iodized oil is partially accumulated is hindered by the partial volume effect or the beam-hardening artifact generated by hyperattenuating iodized oil (4), and this could subsequently result in a false-positive or false-negative diagnosis.

With the introduction of dual energy CT (DECT), several recent studies have focused on the potential clinical applications of DECT in the abdomen according to the finding that the attenuation value of iodinated contrast material is greater at 80 kVp than at 120 kVp or 140 kVp because of the greater photoelectric absorption and lower Compton scatter (11-17).

Based on several studies in which the DECT data set could be preferentially used for evaluating focal hepatic lesions (12, 13, 16, 18), we postulated that various image fusion techniques with DECT could provide more valuable images to detect the residual viable tumor or recurrent tumor within or around the iodized oil-retaining tumor. However, to the best of our knowledge, few reports have been presented in which different blending methods have been compared with respect to the evaluation of HCC after TACE.

The purpose of our study was to compare the linear blending image with the nonlinear moidal blending image of dual energy CT for the evaluation of the viable portion of HCC after TACE.

MATERIALS AND METHODS

Patient Population

Our institutional review board approved this retrospective study and the requirement for informed consent was waived. Between December 2009 and January 2011, through a search of the database of our hospital, a total of 450 consecutive patients who underwent various TACE sessions for the management of HCC were included in this study. Of them, 369 patients were excluded from this study for the following reasons: 1) Multiphasic CT scanning was performed using CT scanners other than a dual-energy CT with which the dual energy mode was applied to the late arterial phase scanning (n = 206). 2) The size of the possible residual or recurrent portions within or around the iodized oil-retaining tumors was too small to be analyzed (an area less than 5 mm^2) (n = 61). 3) The presence of tumoral enhancement within or around the iodized oil-retaining tumor was not confirmed according to the angiography (n = 49). 4) CT images revealed that HCCs were completely treated; that is, only HCCs with compact accumulation in terms of the accumulation pattern of iodized oil were present within the mass on the CT images (n = 35). 5) HCC was diffusely infiltrating throughout the entire liver (n = 10). 6) The absence of tumoral enhancement within or around the iodized oil-retaining tumor was confirmed according to the angiography (n = 8). The remaining 81 patients (66 men and 15 women, age range: 44-88 years, mean age: 64 years) with 123 lesions were finally enrolled in this study.

All 123 lesions showed either a partial defect or faint accumulation in terms of the accumulation pattern of iodized oil within the mass on the CT images. Fifty-three patients had one HCC, 19 patients had two HCCs and 9 patients had more than three HCCs (six patients with three lesions, two patients with four lesions, one patient with six lesions). The mean diameter of the HCCs encompassing both the iodized oil-retaining portions and the residual or recurrent portions was 2.8 ± 1.1 cm (standard deviation) (range: 1.3-5.3 cm). All the patients were diagnosed as having liver cirrhosis. The etiology of liver cirrhosis was as follows; hepatitis B (n = 47), hepatitis C (n = 11), hepatitis B and C (n = 1), and idiopathic (n = 22). The diagnosis of the viable portion within or around the iodized oil-retaining tumor was made by a subsequent angiography after multiphasic CT scanning using a dual-energy CT (n = 123) or typical imaging findings (arterial enhancement in the late arterial phase followed by wash-out in the portal/delayed phase) on dynamic contrast-enhanced MRI (n = 28) according to the American Association for the Study of Liver Disease (19). All the patients

were regularly monitored with follow-up CT examinations (one month after TACE procedure and every 3 months thereafter) until the recurrent HCC was detected. The mean interval between the last TACE and the follow-up CT examination using a dual-energy CT that was reviewed in this study was 65 ± 55 days (range: 25-386 days).

The mean body mass index for all the patients was 23.9 ± 2.5 kg/m^2 (standard deviation) (range: 17.5-32.1 kg/m^2). There was only one patient whose body mass index was greater than 30.

CT Examination

CT scanning was performed using a dual-energy CT scanner (Somatom Definition Flash; Siemens Healthcare, Forcheim, Germany). Unenhanced CT was initially performed from the hepatic dome to the renal hilum. These images were used as a baseline study to evaluate the degree of contrast enhancement of the viable portion of HCC on the contrast-enhanced CT images. The unenhanced CT images were obtained with 4-mm collimation and a 4-mm reconstruction interval. Triple phase (the late arterial, portal venous and delayed phases) contrast-enhanced CT was performed after intravenous injection of 100-150 mL of iodinated contrast material with a power injector (Medrad Stellant Dual Head Injector; Medrad, Warrendale, PA, USA) at a rate of 3 mL/sec through an antecubital vein. The 80 kVp and Sn140 kVp images were acquired in the late arterial phase, while only the 120 kVp images were acquired in the portal venous and delayed phases. A higher tube current (quality reference mAs: 200) was selected for the 80 kVp setting to reduce the image noise. The tube current setting (quality reference mAs: 77) for the Sn140-kVp setting was automatically preset by the software. The scanning parameters used for the late arterial phase imaging were as follows: a detector configuration of 32 × 0.6, a gantry rotation time of 0.5 sec, a pitch of 0.8 and the use of a D26f medium kernel. CT scanning was performed with the patient in the supine position and automated tube current modulation (Care Dose 4D, Siemens Healthcare, Erlargen, Germany) was routinely used. The scan delay was according to an automatic bolus triggering software program (Syngo Acquisition Workplace; Siemens Healthcare, Erlargen, Germany). The late arterial phase scanning and portal venous phase scanning were started at 18 and 55 seconds, respectively, after the trigger threshold [100 Hounsfield units (HUs) on the abdominal aorta] was reached. The delayed phase scanning was performed 180 seconds after the initiation of the contrast material injection. The scan range was from the diaphragmatic dome to the hepatic angle for the late arterial and delayed phase scanning, while in the portal venous phase scanning, the CT images were obtained from the diaphragmatic dome to the symphysis pubis. The patients were exposed to an average dose of radiation during precontrast, late arterial, portal venous and delayed phase CT scanning of 2.75, 2.91, 5.54 and 2.64 mSv, respectively.

The linear blending and moidal blending images during the late arterial phase were obtained using dual energy post-processing software (Syngo MMWP, VE36A; Siemens Healthcare, Erlargen, Germany) by an experienced technician. It took approximately 1.5 and 3 minutes on average to reconstruct the linear blended and moidal, blended images, respectively. The linear blended image was generated as a result of blending the Sn140 kVp and 80 kVp data sets with the weighting factor of 0.5. The effect of the moidal blending function on the DECT datasets can be modulated by two parameters: the blending level (λ) and the blending width (ω). In order to generate the moidal blended image, the blending center and the blending width were set to 100 HU and 400 HU, respectively, based on previous studies (13, 20).

Quantitative Analysis

An abdominal radiologist with 5 years experience performed quantitative measurements with respect to both the linear blending and moidal blending images at a Picture Archiving and Communication System (PACS) monitor (PACS; Marotech 5.4, Seoul, Korea). The mean CT numbers (as expressed in HUs) of the remnant or recurred viable portion within or around the iodized oil-retaining tumor were measured using circular regions of interest (ROIs). Because the viable portion was adjacent to the iodized oil-retaining portion in most cases, special care was given in order to avoid including the hyper-attenuating iodized oil-retaining portion when manually placing the ROIs within the hypervascular viable portion. The size of the ROI varied according to the size of the viable portion and the ROI was made to cover as much of the hypervascular enhancing portion as possible [mean size: 13.1 ± 2.5 mm^2 (standard deviation), range: 5.1-54.3 mm^2]. The mean CT numbers of the hepatic parenchyma were also obtained using circular ROIs, the size of

which was 50 mm^2. The ROI was placed over the liver parenchyma while avoiding the large vessels and the regions with focal changes of the hepatic parenchymal density. In order to measure the image noise, a circular ROI (50 mm^2 in size) was placed in the subcutaneous fatty layer of the anterior abdominal wall. The standard deviation of the measurement was defined as the image noise. The ROI was measured three times at different locations and the mean value of the three measurements was used for the statistical analysis. The lesion-to-liver contrast-to-noise ratio (CNR) was calculated with respect to the background noise by using the following formula: $CNR = (ROI_{lesion} - ROI_{liver}) / SD_{noise}$, where ROI_{lesion} is the mean CT number of the hypervascular viable portion of the tumor, ROI_{liver} is the mean CT number of the background liver and SD_{noise} is the standard deviation of the subcutaneous fat.

Qualitative Analysis

An abdominal radiologist with 9 years experience and a third-year resident independently analyzed the linear blending and moidal blending images at a PACS monitor (PACS; Marotech 5.4, Seoul, Korea). Each image set, which consisted of the pre-contrast image, the contrast-enhanced late arterial, portal and delayed phase images, was presented in two separate reading sessions to both reviewers. To minimize the recall bias, each reading session was separated by 4 weeks. The cases were randomly presented in each session. The patient's information such as name, age, gender and hospital record number, and the CT parameters were omitted from the images. Both reviewers were aware of the location of the tumor in the liver and the size of each lesion and they evaluated the images in a stack mode. The readers were allowed to adjust the window width and level to suit their preference. The reference criteria for the five point scales used for qualitative assessment were established by consensus by both reviewers in advance of image analysis. Each reviewer assessed the lesion conspicuity on two blending images using five-point ordinal scales (1 = non-visible, 2 = barely visible, 3 = subtle but detectable, 4 = easily detectable, 5 = obviously visible). The lesion conspicuity was classified as 'non-visible' when there was no visual perception of arterial tumoral enhancement within or around the iodized oil-retaining tumor. It was classified as 'barely visible' when the viable tumor portion had a higher attenuation on an arterial phase image than on a pre-contrast image, but had lower attenuation than the liver parenchyma on an arterial phase image. The lesion conspicuity was classified as 'subtle but detectable' when the viable tumor portion had a higher attenuation on an arterial phase image than on a pre-contrast image but had similar attenuation as the liver parenchyma on an arterial phase image. It was regarded as 'easily detectable' when the viable tumor portion had higher attenuation than the liver parenchyma on an arterial phase image. The lesion conspicuity was considered to be 'obviously visible' when the viable tumor portion had similar attenuation as the hepatic artery on an arterial phase image. Both reviewers also evaluated both blending images using a five-point scale with respect to the image sharpness (1 = marked blurring of organ contours, 2 = below average, 3 = average, 4 = above average, 5 = sharpest delineation of organ contours), image noise level (1 = minimal or absent, 2 = below average, 3 = average noise in an acceptable image, 4 = above average, 5 = unacceptable) and overall image quality (1 = non-diagnostic, 2 = suboptimal, 3 = fair, 4 = good, 5 = excellent). The image sharpness was regarded as a 'marked blurring of organ contours' when the outer margin of the upper abdominal organs appeared as more than double lines. It was regarded as 'average' when the outer margin of the upper abdominal organs appeared as a blunt single line. The image sharpness was regarded as 'sharpest delineation of organ contours' when the outer margin of the upper abdominal organs appeared as a sharp single line. It was considered as 'below average' when the image sharpness was between 'marked blurring of organ contours' and 'average'. The image sharpness was considered 'above average' when the image sharpness was between 'average' and 'sharpest delineation of organ contours'. The image noise was regarded as 'minimal or absent' when mottling was at minimal or less than perceptible levels. It was regarded as 'average noise in an acceptable image' when there was an average amount of mottles and satisfactory perception of small anatomic structures such as blood vessels. The image noise was regarded as 'unacceptable' when the number of mottles interfered with the perception of small anatomic structures such as blood vessels. It was considered 'below average' when the amount of image noise was between 'minimal or absent' and 'average noise in an acceptable image'. The image noise was considered 'above average' when the amount of the image noise was between 'average noise in an acceptable image' and 'unacceptable'. The overall

image quality was graded based on the reviewers' subjective evaluation of the image. The overall image quality was regarded as 'non-diagnostic' when the impression of the image quality was too poor to evaluate the focal hepatic lesion. It was regarded as 'suboptimal' when the impression of image quality was markedly inferior to the standard live CT image using 120 kVp. The overall image quality was regarded as 'fair' when the impression of image quality was slightly inferior to the standard live CT image using 120 kVp. It was regarded as 'good' when the impression of image quality was equivalent to the standard live CT image using 120 kVp. The overall image quality was regarded as 'excellent' when the impression of image quality was superior to the standard live CT image using 120 kVp.

Statistical Analysis

All the statistical analyses were performed with commercially available software (SPSS for Windows, version 18, SPSS, Chicago, IL, USA). Statistical significance was considered to be present when the *p* value was below 0.05. The paired *t*-test was used to compare the lesion-to-liver CNR and the image noise between the linear blending and moidal blending images. The lesion conspicuity, image sharpness, image noise and overall image quality were compared for both blending images by the Wilcoxon matched-pair signed-ranks test. The degree of interobserver agreement with respect to the qualitative analysis was categorized in terms of weighted kappa values as less than 0.20 (poor agreement), 0.21-0.40 (fair agreement), 0.41-0.60 (moderate agreement), 0.61-0.80 good agreement and greater than 0.81 (excellent agreement).

RESULTS

Quantitative Analysis

There was a statistically significant difference for both the attenuation value of the lesion and image noise between two blending images ($p < 0.001$). The mean attenuation value of the remnant or recurred viable portion within or around the iodized oil-retaining tumor for the linear blending and moidal blending images was 116.2 ± 19.5 HU and 129.8 ± 24.1 HU, respectively. The linear blending image showed increased image noise (mean value: 17.5 ± 5.5 HU, range: 6.1-34.1 HU) compared with the moidal blending image (mean value: 10.9 ± 3.5 HU, range: 3.2-23.8 HU). However, with respect to the attenuation value of the background liver parenchyma, there was no significant difference between the two blending images (74.0 ± 11.4 HU for the linear blending image and 75.0 ± 12.3 HU for the moidal blending image). The mean lesion-to-liver CNR for the viable portion of the tumor was 2.7 ± 1.6 for the linear blending image and 5.6 ± 3.2 for the moidal blending image, which showed a statistically significant difference ($p < 0.001$) (Table 1).

Qualitative Analysis

The results of visual comparison between the two blending images with regard to lesion conspicuity, image sharpness, image noise and overall image quality are summarized in Table 2. Both reviewers' scores of the conspicuity of the hypervascular viable portion within or around the iodized oil-retaining tumor increased significantly for the moidal blending image (reviewer 1: 4.3 ± 0.8, reviewer 2: 4.6 ± 0.7) compared with the linear blending image (reviewer 1: 3.8 ± 1.1, reviewer 2: 3.7 ± 1.1) ($p < 0.001$) (Fig. 1). Both reviewers rated the linear blending image as having more image noise (reviewer 1: 3.7 ± 0.7, reviewer 2: 3.8 ± 0.6) than the moidal blending image (reviewer 1: 2.7 ± 0.9, reviewer 2: 2.3 ± 0.8) ($p < 0.001$). The analysis of the visual grading of the overall image quality showed that the readers' rankings were significantly higher for the moidal blending image (reviewer 1: 3.6 ± 0.7, reviewer 2: 4.0 ± 0.5) compared with the linear blending image (reviewer 1: 3.3 ± 0.7, reviewer 2: 3.1

Table 1. Comparison of the Attenuation Values of the Lesions and Liver Parenchyma, the Image Noise and the Lesion-to-Liver CNR between the Linear Blending and Moidal Blending Images

Parameter	Linear Blending	Moidal Blending	*p* Value
Attenuation value of the lesions (HU)	116.2 ± 19.5	129.8 ± 24.1	< 0.001
Attenuation value of the background liver (HU)	74.0 ± 11.4	75.0 ± 12.3	0.238
Image noise (HU)	17.5 ± 5.5	10.9 ± 3.5	< 0.001
Lesion-to-liver CNR	2.7 ± 1.6	5.6 ± 3.2	< 0.001

The data is expressed as mean ± standard deviations.
Note.—CNR = contrast-to-noise ratio, HU = Hounsfield unit

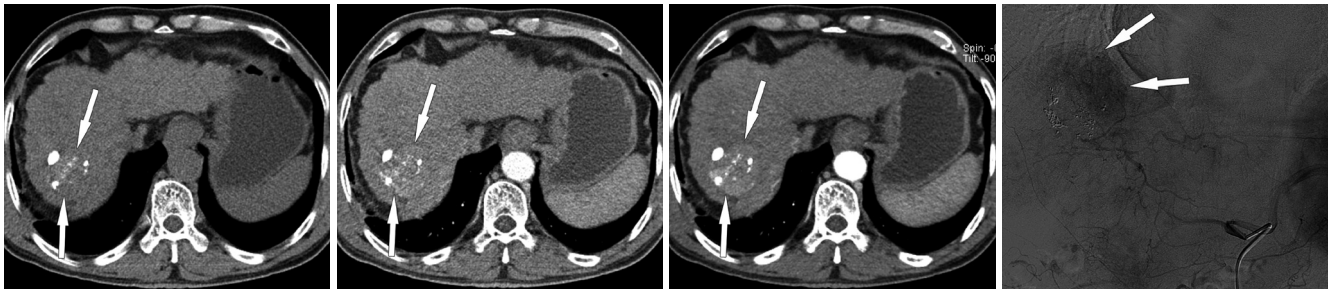

A B C D

Fig. 1. A 59-year-old man who underwent two sessions of transcatheter arterial chemoembolization for HCC.
A. The unenhanced CT image shows a sparsely iodized oil-retaining lesion at the right hepatic dome (arrows).
B. The linear blending image obtained during the late arterial phase shows a questionable area of enhancement (arrows) within a sparsely iodized oil-retaining lesion at the right hepatic dome.
C. The moidal blending image obtained during the late arterial phase more clearly demonstrates the hypervascular enhancing portion (arrows) within a sparsely iodized oil-retaining lesion at the right hepatic dome.
D. The celiac axis angiogram reveals hypervascular staining (arrows) fed by branches of the right hepatic artery at the right hepatic dome.
Note.—HCC = hepatocellular carcinoma

Table 2. Comparison of Qualitative Assessment between the Linear Blending and Moidal Blending Images

Parameter	Reviewer 1			Reviewer 2		
	Linear Blending	Moidal Blending	*p* Value	Linear Blending	Moidal Blending	*p* Value
Lesion conspicuity	3.8 ± 1.1	4.3 ± 0.8	< 0.001	3.7 ± 1.1	4.6 ± 0.7	< 0.001
Image sharpness	4.1 ± 0.5	3.8 ± 0.6	< 0.001	4.0 ± 0.5	3.9 ± 0.7	< 0.01
Image noise	3.7 ± 0.7	2.7 ± 0.9	< 0.001	3.8 ± 0.6	2.3 ± 0.8	< 0.001
Overall image quality	3.3 ± 0.7	3.6 ± 0.7	< 0.001	3.1 ± 0.5	4.0 ± 0.5	< 0.001

Note.—HCC = hepatocellular carcinoma

Table 3. Inter-Observer Agreement between the Two Reviewers

Parameter	Kappa Value for the Linear Blending Image	Kappa Value for the Moidal Blending Image
Lesion conspicuity	0.685	0.590
Image sharpness	0.493	0.479
Image noise	0.631	0.529
Overall image quality	0.426	0.396

± 0.5) for both readers ($p < 0.001$). In contrast, with respect to the image sharpness, the reviewers' rankings were significantly higher for the linear blending image (reviewer 1: 4.1 ± 0.5, reviewer 2: 4.0 ± 0.5) than for the moidal blending image (reviewer 1: 3.8 ± 0.6, reviewer 2: 3.9 ± 0.7) for both reviewers ($p < 0.01$). In respect to the interobserver agreement, the weighted kappa values ranged from 0.396 to 0.685 (Table 3).

DISCUSSION

The DECT scanner has two X-ray tubes and the corresponding detectors are placed in an orthogonal geometry, thus allowing for simultaneous dual-energy scanning (20). The ability of DECT to perform 80 kVp scanning has been expected to be beneficial for evaluating hypervascular hepatic tumors because a low tube voltage scan was reported to have a better CNR and conspicuity than a high voltage scan (13, 15). However, the use of low-kV scanning is accompanied by increased image noise, and this may decrease the overall image quality. In an effort to reduce the increased noise of low-kV images, several methods for blending both the DECT data sets at two photon energies have been developed (12, 20). That is, through image blending, it is possible to combine the advantages of both the 80 kVp and 140 kVp data, while the disadvantages of each type of data set are minimized.

Historically, the linear blending method was initially used to produce fused 140-kV and 80-kV scans, and the weighting factor can be selected between 0 and 1. The linear blended image with a weighting factor of 0.3 (70% of the fused image information from the 140 kVp image and 30% from the 80 kVp image) is regarded as a routine reconstruction image because it has approximately similar image characteristics as those of a standard 120 kVp single energy scan (12, 21, 22). However, in the case of the Somatom Definition Flash CT scanner, a weighting factor of 0.4 needs to be used in order to produce images that are sim-

ilar to a standard 120 kVp image due to the presence of a tin filter in the 140 kVp tube; this weighting factor is based on the manufacturer's recommendation. According to several previous studies that compare different weighting factors (11, 13, 23), although the image noise increases in proportion to a weighting factor, weighting factors greater than 0.5 produce fusion images with a higher CNR and superior image quality. Thus, in this study, we adopted a weighting factor of 0.5 as an optimal parameter for the linear blended image.

Continued refinement has been made of the non-linear blending techniques to maximize the advantages of both energy data sets, although the linear blended image provides some improvement in contrast resolution along with decreased noise. For example, the moidal blending method uses a flexible mixing ratio depending on the HU values of the voxels (20). That is, high contrast resolution with less noise could be accomplished through a preferential blending function on each voxel basis. The two parameters (the blending level and the blending width) have a direct effect on the moidal blended image. As the level (λ) increases, the effect of the 80 kVp image on a voxel with a given CT number decreases, while as the width (ω) increases, the rate of change in transition from a low contribution of the 80 kVp image to a high contribution of the 80 kVp image decreases (13). Based on the previous experimental and clinical data, which suggested that it would be desirable to set λ and ω at a value between the hypervascular lesion and the background liver, respectively, and to set the value as wide as possible (13, 20), we used 100 and 400 HU as the λ and the ω values, respectively.

Our study showed that the moidal blending method using the Sn140 kVp and 80 kVp images with DECT could significantly improve the conspicuity of tumoral enhancement within or around the iodized oil-retaining tumor, together with superior overall image quality, compared with the linear blending method. In our study, the CNR of the viable portion of HCC after TACE increased more than two times when the moidal blended image was compared with the linear blended image. This result seems to reflect the fact that the moidal blending function differentially weighs voxels with the low HU values toward the 140 kVp data set and the voxels with the high HU values are weighted toward the 80 kVp data set (20). That is, voxels of the hypervascular viable portion of HCC in the moidal blended image can be interpreted to mainly come from the 80 kVp data set. This could explain the result of our study which suggests that the mean attenuation value of the lesions was significantly greater on the moidal blended image than on the linear blended image. In contrast, the mean values of the background liver parenchyma were nearly similar between the two blended images. Given that the value of level (λ) was set between the mean attenuation values of the viable portion and the background liver, we believe that the moidal blended image in our study was generated with optimally selected parameters, and this could result in significant improvement over the image made by the linear blended technique with respect to lesion conspicuity and the overall image quality. These results are supported by those of the previous studies (13, 20).

Regarding image noise, our results differ from those of the previous study by Kim et al. (13). While Kim et al. reported that image noise on the moidal blended images was either comparable to or greater than that on the linear blended images with various weighting factors, in our study, the image noise was significantly increased on the linear blended image. This discrepancy in image noise might be attributable to the differences in parameters used for the moidal blending technique, the CT scanner used and the structure of the 140 kVp tube.

Both reviewers, in our study, considered the linear blended image to have better image sharpness than the moidal blended image, which could mean that there was a perceptible loss of anatomic structure delineation to some degree. However, the moidal blended image showed superior lesion conspicuity, together with decreased image noise. Thus, it is assumed that there could be a trade-off between the benefits of superior lesion conspicuity and noise reduction, and the risk of a loss of spatial resolution during the reconstruction of the moidal blended image. Nevertheless, given the moidal blended image was considered to show superior overall image quality, we believe that the readers tended to prefer images with better contrast at the expense of decreased spatial resolution.

The residual or locally recurrent tumor should be detected as soon as possible on a series of follow-up CT examinations after TACE in order to provide the chance for the tumor to be successfully managed at an early stage of HCC. Because iodine enhancement within or around the iodized oil-retaining tumor during the hepatic arterial phase is the most distinguishing feature indicative of a viable portion of HCC, the greater contrast

resolution could lead to a greater chance to correctly detect the viable portion of HCC. From this point of view, the ability of the moidal blended CT images to achieve a better CNR during the hepatic arterial phase may be beneficial to evaluate a questionable area of enhancement on the follow-up CT after TACE. It is also assumed that the improved lesion-to-liver contrast of the moidal blended images may be effectively used to overcome the limitations of a CT examination as any arterial enhancing viable portion of HCC after TACE may be obscured by the high attenuation density of the iodized oil. This suggestion, however, needs to be further validated by subsequent studies.

This study has several limitations. First, in our study we did not compare various combinations of parameters in fused images. Instead, we adopted linear and nonlinear moidal blending methods with fixed parameters. We considered that the parameters used in our study could produce the representative images of both blending methods, as based on previous studies. Second, the value of the 80 kVp and 140 kVp images as well as the iodine map were not evaluated for the detection of the viable portion of HCC. Third, there may be an intrinsic selection bias because we had included only those patients in whom a residual or recurrent tumor was confirmed with angiography or MRI. Fourth, only one patient had a body mass index greater than 30 in our patient population. Thus, the results of our study need to be cautiously interpreted especially for obese patients.

In conclusion, the nonlinear moidal blending image of dual energy CT showed an increased lesion-to-liver CNR, decreased noise and improved overall image quality for the evaluation of the viable portion of HCC after TACE.

REFERENCES

1. Kim KW, Lee JM, Choi BI. Assessment of the treatment response of HCC. *Abdom Imaging* 2011;36:300-314
2. Kim S, Mannelli L, Hajdu CH, Babb JS, Clark TW, Hecht EM, et al. Hepatocellular carcinoma: assessment of response to transarterial chemoembolization with image subtraction. *J Magn Reson Imaging* 2010;31:348-355
3. Lim HS, Jeong YY, Kang HK, Kim JK, Park JG. Imaging features of hepatocellular carcinoma after transcatheter arterial chemoembolization and radiofrequency ablation. *AJR Am J Roentgenol* 2006;187:W341-W349
4. Yu JS, Kim JH, Chung JJ, Kim KW. Added value of diffusion-weighted imaging in the MRI assessment of perilesional tumor recurrence after chemoembolization of hepatocellular carcinomas. *J Magn Reson Imaging* 2009;30:153-160
5. Llovet JM, Real MI, Montaña X, Planas R, Coll S, Aponte J, et al. Arterial embolisation or chemoembolisation versus symptomatic treatment in patients with unresectable hepatocellular carcinoma: a randomised controlled trial. *Lancet* 2002;359:1734-1739
6. Lo CM, Ngan H, Tso WK, Liu CL, Lam CM, Poon RT, et al. Randomized controlled trial of transarterial lipiodol chemoembolization for unresectable hepatocellular carcinoma. *Hepatology* 2002;35:1164-1171
7. Belghiti J, Carr BI, Greig PD, Lencioni R, Poon RT. Treatment before liver transplantation for HCC. *Ann Surg Oncol* 2008;15:993-1000
8. Kubota K, Hisa N, Nishikawa T, Fujiwara Y, Murata Y, Itoh S, et al. Evaluation of hepatocellular carcinoma after treatment with transcatheter arterial chemoembolization: comparison of Lipiodol-CT, power Doppler sonography, and dynamic MRI. *Abdom Imaging* 2001;26:184-190
9. Jang KM, Choi D, Lim HK, Lim JH, Lee JY, Lee WJ, et al. Depiction of viable tumor in hepatocellular carcinoma treated with transarterial chemoembolization: multiphasic helical CT with review of the previous serial CT images. *Korean J Radiol* 2005;6:153-160
10. Lau WY, Lai EC. Hepatocellular carcinoma: current management and recent advances. *Hepatobiliary Pancreat Dis Int* 2008;7:237-257
11. Behrendt FF, Schmidt B, Plumhans C, Keil S, Woodruff SG, Ackermann D, et al. Image fusion in dual energy computed tomography: effect on contrast enhancement, signal-to-noise ratio and image quality in computed tomography angiography. *Invest Radiol* 2009;44:1-6
12. Fletcher JG, Takahashi N, Hartman R, Guimaraes L, Huprich JE, Hough DM, et al. Dual-energy and dual-source CT: is there a role in the abdomen and pelvis? *Radiol Clin North Am* 2009;47:41-57
13. Kim KS, Lee JM, Kim SH, Kim KW, Kim SJ, Cho SH, et al. Image fusion in dual energy computed tomography for detection of hypervascular liver hepatocellular carcinoma:

phantom and preliminary studies. *Invest Radiol* 2010;45:149-157
14. Macari M, Spieler B, Kim D, Graser A, Megibow AJ, Babb J, et al. Dual-source dual-energy MDCT of pancreatic adenocarcinoma: initial observations with data generated at 80 kVp and at simulated weighted-average 120 kVp. *AJR Am J Roentgenol* 2010;194:W27-W32
15. Marin D, Nelson RC, Samei E, Paulson EK, Ho LM, Boll DT, et al. Hypervascular liver tumors: low tube voltage, high tube current multidetector CT during late hepatic arterial phase for detection--initial clinical experience. *Radiology* 2009;251:771-779
16. Robinson E, Babb J, Chandarana H, Macari M. Dual source dual energy MDCT: comparison of 80 kVp and weighted average 120 kVp data for conspicuity of hypo-vascular liver metastases. *Invest Radiol* 2010;45:413-418
17. Sommer CM, Schwarzwaelder CB, Stiller W, Schindera ST, Heye T, Stampfl U, et al. Dual-energy computed-tomography cholangiography in potential donors for living-related liver transplantation: initial experience. *Invest Radiol* 2010;45:406-412
18. Coursey CA, Nelson RC, Boll DT, Paulson EK, Ho LM, Neville AM, et al. Dual-energy multidetector CT: how does it work, what can it tell us, and when can we use it in abdominopelvic imaging? *Radiographics* 2010;30:1037-1055
19. Bruix J, Sherman M; American Association for the Study of Liver Diseases. Management of hepatocellular carcinoma: an update. *Hepatology* 2011;53:1020-1022
20. Holmes DR 3rd, Fletcher JG, Apel A, Huprich JE, Siddiki H, Hough DM, et al. Evaluation of non-linear blending in dual-energy computed tomography. *Eur J Radiol* 2008;68:409-413
21. Schindera ST, Nelson RC, Mukundan S Jr, Paulson EK, Jaffe TA, Miller CM, et al. Hypervascular liver tumors: low tube voltage, high tube current multi-detector row CT for enhanced detection--phantom study. *Radiology* 2008;246:125-132
22. Graser A, Johnson TR, Chandarana H, Macari M. Dual energy CT: preliminary observations and potential clinical applications in the abdomen. *Eur Radiol* 2009;19:13-23
23. Paul J, Bauer RW, Maentele W, Vogl TJ. Image fusion in dual energy computed tomography for detection of various anatomic structures--effect on contrast enhancement, contrast-to-noise ratio, signal-to-noise ratio and image quality. *Eur J Radiol* 2011;80:612-619

경도관동맥화학색전술로 치료받은 간세포암의 평가에 있어 이중에너지 CT: 선형혼합기법과 비선형 Moidal 기법의 비교[1]

신상수[1] · 강형근[2] · 김형욱[1] · 김진웅[2] · 허숙희[2] · 정용연[2] · 선현주[2] · 이다운[1]

목적: 경도관동맥화학색전술(transcatheter arterial chemoembolization; 이하 TACE) 후 잔류 종양이 있는 간세포암의 평가에 있어 이중에너지 CT로 얻은 선형혼합영상과 비선형 moidal 혼합 영상을 비교하고자 하였다.

대상과 방법: TACE 후 불완전 치료가 된 123예의 간세포암을 대상으로 하였다. 이중에너지 모드(80 kVp와 Sn140 kVp)는 후기 동맥기 영상을 얻을 때 적용하였다. Paired *t*-test를 사용하여 두 영상 사이에 병변대 간의 신호대잡음비와 영상잡음을 비교하였다. 병변의 명확도, 영상의 선명도, 영상잡음, 전체적인 영상의 질은 Wilcoxon matched-pair signed-ranks test를 사용하여 비교하였다.

결과: 병변대 간의 신호대잡음비는 선형혼합영상(2.7 ± 1.6)에 비해 moidal 혼합영상(5.6 ± 3.2)에서 유의하게 높았다($p < 0.001$). 영상잡음은 선형혼합영상(17.5 ± 5.5)에 비해 moidal 혼합영상(10.9 ± 3.5)에서 유의하게 낮았다($p < 0.001$). 병변의 명확도, 전체적인 영상의 질은 moidal 혼합영상에서 더 좋았다($p < 0.001$). 그러나, 영상의 선명도는 선형혼합영상이 더 좋았다($p < 0.01$).

결론: TACE 후 잔류 종양이 있는 간세포암의 평가에 있어 이중에너지 CT로 얻은 비선형 moidal 혼합영상은 선형혼합영상에 비해 병변대 간의 신호대잡음비, 영상잡음, 전체적인 영상의 질이 우수하였다.

[1]전남대학교 의과대학 전남대학교병원 영상의학과, [2]전남대학교 의과대학 화순전남대학교병원 영상의학과